Slow relaxation in structure-forming ferrofluids

Aparna Sreekumari* and Patrick Ilg
Polymer Physics, Department of Materials, ETH Zürich, Wolfgang-Pauli Strasse 10, CH-8093 Zürich, Switzerland
(Received 19 August 2013; published 30 October 2013)

We study the behavior of colloidal magnetic fluids at low density for various dipolar interaction strengths by performing extensive Langevin dynamics simulations with model parameters that mimic cobalt-based ferrofluids used in experiments. Our study mainly focuses on the structural and dynamical properties of dipolar fluids and the influence of structural changes on their dynamics. Drastic changes from chainlike to networklike structures in the absence of an external magnetic field are observed. This crossover plays an important role in the slowing down of dynamics that is reflected in various dynamical properties including the tracer diffusion and the viscosity and also in the structural relaxation.

DOI: 10.1103/PhysRevE.88.042315 PACS number(s): 82.70.Dd, 75.50.Mm, 75.75.Jn, 61.20.Ja

I. INTRODUCTION

Ferrofluids are colloidal suspensions of ferromagnetic nanoparticles that are stabilized against agglomeration by coating with surfactants or by surface charges. The change in physical properties of ferrofluids, with an externally applied magnetic field, has several technological and medical applications [1,2]. Thus, there is an evolving interest in understanding the influence of dipolar interactions and magnetic fields on the structure and dynamics of ferrofluids and the phase transitions. The structure and phase behavior of ferrofluids is determined by steric repulsion, attractive van der Waals interactions, and dipole-dipole interactions, which are anisotropic in nature [3,4].

For the zero-field case, in the regime of low magnetic interaction strength (with negligible anisotropic interactions), the structure and phase behavior are determined by attractive and repulsive interactions in the system [5]. For repulsive systems, a fluid-solid-like phase transition is expected with no critical point [6]. For attractive systems, the phase diagram is very rich, containing a fluid-solid phase transition, a liquid-gas phase transition, and an associated critical point that has been well studied [7].

In the case of high magnetic interaction strengths, the classical work of de Gennes and Pincus [8] has shown that ferrofluids having strong dipolar strength are inclined to form clusters and chains depending on the density of the system. Various theoretical studies have attempted to understand the chain formation in dipolar fluids either with straight and rigid chain models [9–14] or with a flexible chain model [15,16] by neglecting interchain interactions. The chain model predicts an exponential decay behavior of the cluster size distribution that has indeed been observed using computer simulations [17–21]. The chain, ring, and other microstructure formation in dipolar fluids is relevant for understanding the phase behavior of the system. The existence of a gas-liquid phase transition in dipolar fluids is still an open question [22–25] in the absence of a magnetic field.

The influence of structural changes on the dynamics of ferrofluids has not been studied systematically in the absence of a magnetic field so far. One of the widely studied dynamic quantities is the self-diffusion (D). The dependence of D on the dipolar interaction strength, volume fraction, and scattering length scale has been reported in previous works [26–29]. The microstructure formation in the system considerably affects the self-diffusion and other dynamic quantities which will be one of the aspects we discuss in the present work. We believe that the dependence of structural changes on dynamics can be used as a tool to understand the origin of anisotropy in the viscosity of ferrofluids in the presence of a weak magnetic field.

The presence of a magnetic field favors chain formation and influences the liquid-gas phase transition [14,22,28,30,31]. Among various properties of ferrofluids, the magnetoviscous effect (MVE) [32], i.e., the change in viscosity with a change in magnetic field, plays an important role in fundamental research due to its many applications ranging from engineering and technology to medical treatments [33–36]. It is an experimentally observed fact that chain-forming ferrofluids show a large MVE [37,38]. The origin of the MVE and its anisotropic behavior with change in the orientation of the magnetic field requires better understanding [39–42].

In this paper, we investigate the zero-field properties of model ferrofluids for parameters that mimic the cobalt-based ferrofluids used in experiments [42]. A systematic study of structural properties and the corresponding changes in dynamics of the system for a range of dipolar interaction strength is presented here. Structural properties characterized by the pair correlation function, the connectivity, the static structure factor, and the cluster size distribution show the formation of complex microstructures constituted of chains and node-forming structures with increase in the dipolar coupling constant. The dynamics of the system has been studied by computing the mean square displacement, the orientational correlation function, the incoherent scattering function, and the stress correlation function. We observe a crossover region in terms of the dipolar interaction strength beyond which the structural and dynamic properties show characteristic changes in their behavior. We provide a comparison of our results with the existing theoretical model to explain the the role of the crossover region in the structural and dynamic transitions.

The paper is organized as follows. The model potentials and equations we use for our simulation study are described in Sec. II. The structural and dynamic properties are explained in Secs. III and IV, respectively. A discussion and conclusions are provided in Sec. V.

*Corresponding author: aparna.sreekumari@mat.ethz.ch

II. MODEL

A. Interaction potential

In the present work, we study model ferrofluid systems where magnetically hard point dipolar particles have short-range repulsive interactions along with long-range dipole-dipole interactions [17,28,40,43–47]. The short-range repulsive interaction mimics the steric repulsion in stabilizing the ferrofluid systems and is given by

$$U_{ij}^{\mathrm{LJ}} = 4\epsilon\left[\left(\frac{\sigma}{r_{ij}}\right)^{12} - \left(\frac{\sigma}{r_{ij}}\right)^{6} - C(r_c)\right], \tag{1}$$

where ϵ is the depth of the potential, r_{ij} is the distance between two particles, and $C(r_c)$ is to ensure continuity at the cutoff of $r_c = 2^{1/6}\sigma$. The long-range dipole-dipole interaction is given by

$$U_{ij}^{\mathrm{dip}} = \frac{\mu_0 m_i m_j}{4\pi r_{ij}^3}[\mathbf{u}_i \cdot \mathbf{u}_j - 3(\mathbf{u}_i \cdot \hat{\mathbf{r}}_{ij})(\mathbf{u}_j \cdot \hat{\mathbf{r}}_{ij})], \tag{2}$$

where $\mathbf{u}_i$ is the orientation and m_i is the magnitude of the magnetic moment of particle i. $\mathbf{r}_{ij} = \mathbf{r}_i - \mathbf{r}_j$ is the connector vector of the two particles, $r_{ij} = |\mathbf{r}_{ij}|$, $\hat{\mathbf{r}}_{ij} = \frac{\mathbf{r}_{ij}}{r_{ij}}$, and $\mu_0 = 4\pi \times 10^{-7}$ H/m. The long-range dipolar interactions are treated with the reaction field (RF) method [48]. In this method, a cavity of radius r_{RF} (here $r_{\mathrm{RF}} = 8.0\sigma$) is defined within which the interactions of dipolar particles are treated explicitly. The particles outside this cavity form a dielectric continuum (ε_s) which develops a reaction field inside the cavity. The strength of the reaction field acting on particle i is given by

$$\boldsymbol{\varepsilon}_i = \frac{2(\varepsilon_s - 1)}{2\varepsilon_s + 1}\frac{1}{r_{\mathrm{RF}}^3}\sum_j \mathbf{m}_j,$$

where the summation extends over molecules inside the cavity. We choose r_{RF} much greater than r_c of the short-range interactions. We have compared the results obtained by the RF method with those of the Ewald sum method [48], both with metallic boundary conditions ($\varepsilon_s \to \infty$) [17]. For the present range of parameters, we find that both methods give identical results within numerical uncertainties. Since we find the RF method to be computationally more efficient than the Ewald sum method, we choose to perform our simulations with the RF method [49].

B. Model equations and parameters

We have performed Langevin dynamics (LD) computer simulations using translational and rotational Langevin equations of motion [48,50] to study the model ferrofluid system, and the equations are given by

$$M\dot{\mathbf{v}}_i = -\xi^{\mathrm{T}}\mathbf{v}_i(t) + \mathbf{f}_i^{\mathrm{B}}(t) + \mathbf{F}_i, \tag{3}$$

$$\mathbf{I}\cdot\dot{\boldsymbol{\omega}}_i = -\xi^{\mathrm{R}}\boldsymbol{\omega}_i(t) + \boldsymbol{\tau}_i^{\mathrm{B}}(t) + \boldsymbol{\tau}_i, \tag{4}$$

where M and $\mathbf{I}$ are the mass and inertia tensor of the particle with linear and angular velocity $\mathbf{v}_i$ and $\boldsymbol{\omega}_i$, respectively, ξ^{T} is the translational friction coefficient, and ξ^{R} is the rotational friction coefficient. For a solvent of viscosity η_s, $\xi^{\mathrm{T}} = 3\pi\eta_s\sigma$ and $\xi^{\mathrm{R}} = \pi\eta_s\sigma^3$. $\mathbf{f}_i^{\mathrm{B}}(t)$ and $\boldsymbol{\tau}_i^{\mathrm{B}}(t)$ are Gaussian random forces and torques. The potential forces and torques are given by $\mathbf{F}_i = -\nabla_{\mathbf{r}_i} U$ and $\boldsymbol{\tau}_i = -\mathcal{L}_i U$, respectively, with $U = \frac{1}{2}\sum_{ij}(U_{ij}^{\mathrm{LJ}} + U_{ij}^{\mathrm{dip}})$ and the rotational operator $\mathcal{L}_i = \mathbf{u}_i \times \frac{\partial}{\partial \mathbf{u}_i}$.

We performed the simulations with the package "Large-scale Atomic/Molecular Massively Parallel Simulator" (LAMMPS) [51]. The dimensionless parameters we used in the ferrofluid study are the magnetic volume fraction $\phi = \rho\pi d_{\mathrm{m}}^3/6$, where ρ is the number density and d_{m} is the magnetic core diameter, and the dipolar interaction strength (dipolar coupling constant), which is given by

$$\lambda = \mu_0 m^2/4\pi k_{\mathrm{B}} T d_{\mathrm{m}}^3, \tag{5}$$

where m is the magnetic dipole moment and T is the temperature. We work with reduced units where we express the different observables in units of energy (ϵ), length (σ), and mass (M).

The LD simulations have been performed with $N = 1000$ spherical particles with diameter σ (monodisperse) keeping the same volume fraction $\phi = 0.007$ as used in the experimental system [42]. We mimic the experimental system by reproducing the magnetization curve of cobalt-based ferrofluids that is used in experiments. The parameters we adopt for mapping are the saturation magnetization and the volume fraction. We find that for the dipolar interaction strength $\lambda = 4.62$ our data from the simulation reproduce the experimental magnetization curve.

The equilibration is judged by looking at the relaxation time obtained from the self-intermediate scattering function. 5×10^6 LD steps were used for equilibration and 6×10^6 LD steps for data production using a time step of $\Delta t = 0.002\tau_{\mathrm{B}}$, where $\tau_{\mathrm{B}} = d_{\mathrm{m}}^3\xi^{\mathrm{T}}/6k_{\mathrm{B}}T$ is the time taken to diffuse the magnetic core diameter d_{m}. We carried out the simulations for four independent samples to get rid of the correlation with the initial configuration and to improve statistics. Some simulations have been performed for different system sizes in order to discuss possible finite-size effects.

III. STRUCTURAL PROPERTIES

We investigate the structural properties for various dipolar coupling constants at a fixed volume fraction ($\phi = 0.007$). The structural properties are characterized by the radial distribution function, the structure factor, the coordination number, and the cluster size distribution. From our analysis, we find interesting structural behavior at high λ values, which we discuss in this section.

A. Radial distribution function

We first analyze the radial distribution function $g(r)$ which is defined as [52]

$$g(r) = \frac{V}{N^2}\left\langle \sum_i \sum_{j\neq i} \delta(\mathbf{r} - \mathbf{r}_{ij}) \right\rangle, \tag{6}$$

where V is the volume of the system. For an isotropic system, $4\pi r^2 \rho g(r) dr$ gives the number of neighbors a reference particle has between r and $r + dr$, where ρ is the number density of the system.

In Fig. 1, we show $g(r)$ obtained from the simulations carried out at different dipolar coupling constants varying

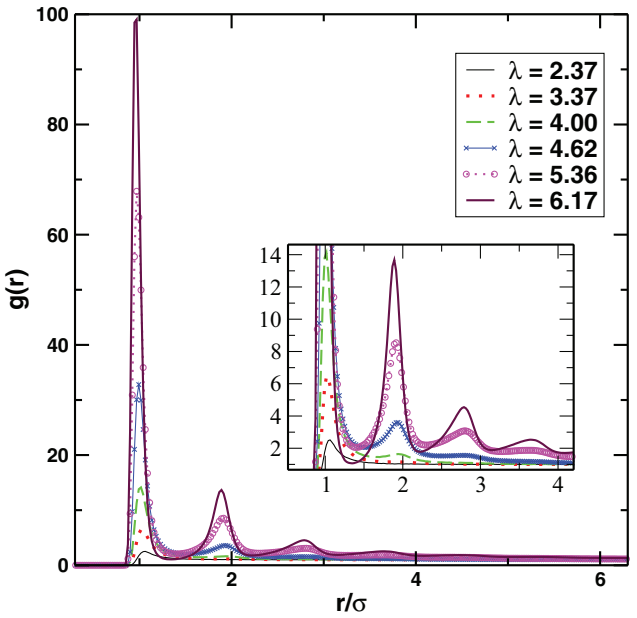

FIG. 1. (Color online) The radial distribution function $g(r)$ at volume fraction $\phi = 0.007$ for systems with different λ values. The inset shows a close-up view of the second, third, and fourth coordination shells.

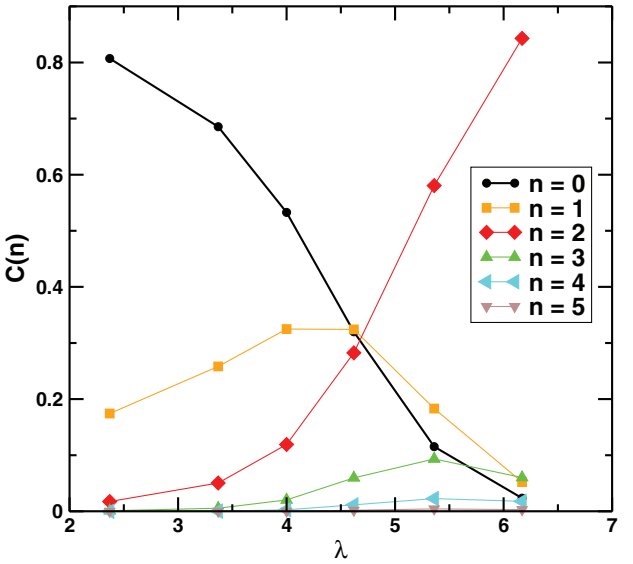

FIG. 2. (Color online) The fraction of particles having coordination number n, $C(n)$, at volume fraction $\phi = 0.007$, for systems with different λ values.

from 2.37 to 6.17. We observe that $g(r)$ shows gaslike behavior at $\lambda = 2.37$ and 3.37 due to weak dipolar interactions. As λ increases further, the system attains a local structural arrangement, which is evident from the peaks in $g(r)$. We find that the amplitude of the sharp first peak increases with λ, indicating a well-defined first coordination shell [17,53,54] due to one-dimensional structure formation. For higher λ values we observe peaks at various length scales, indicating a structural rearrangement beyond the first coordination shell. As we increase interaction strength, around $\lambda = 4.62$, $g(r)$ shows a well-defined second peak corresponding to the second coordination shell as well as a growing third peak, which exhibits the increase in local ordering of the system as λ increases. A recent study on the structure of dipolar hard sphere fluids shows a monotonic decrease in the first minimum of $g(r)$ with decreasing temperature (or increasing λ) [55]. We observe a nonmonotonic behavior in the first minima of $g(r)$ after crossing $\lambda \approx 4.62$, which we consider as the crossover λ value, λ_t. The well-defined first minimum in $g(r)$ is due to the ordering of particles in the system; in our case chain formation causes the well-defined minimum and it is prominent for all higher interaction strengths from λ_t on. The shifting of the first minimum towards shorter distances indicates the presence of connected chains, due to which the second peak of $g(r)$ starts around 1.4σ. We study the structural crossover from disordered to ordered structures at this particular value of λ (λ_t) in detail with the help of other structural properties.

B. Connectivity

The fraction of particles having coordination number n, $C(n)$, is a measure of the local connectivity of the system. Here, two particles are considered to be neighbors if they are closer than a distance 1.5σ. Figure 2 shows that in the weakly interacting regime, the majority are isolated particles; only a few one-coordinated and two-coordinated particles are present. The error bars are of the symbol size if not shown. With increasing λ, the fraction of one-coordinated and two-coordinated particles increases at the expense of isolated particles and at $\lambda_t = 4.62$, the probabilities of finding isolated, one-, and two-coordinated particles are almost equal. Beyond λ_t, the fraction of two-coordinated particles keeps on increasing at the cost of isolated and one-coordinated particles, which explains the presence of chains in the system. We also observe a slight increment in the number of three- and four- coordinated particles which shows the presence of more complicated and multiply connected structures in the system. Such properties in connectivity have been observed in colloidal gels and gel-forming systems [53,54,56].

This structural quantity clearly shows the transformation of a system with mainly isolated particles to chainlike and then to networklike structures with increasing λ. We have checked the results for different bonding criteria based on distances ($r_c = 1.3$–1.6) for higher λ values ($\lambda = 5.37$ and 6.17). We have observed only a small quantitative change in the connectivity as we change the bonding criteria. Since our choice is $r_c = 1.5$ and the minimum of $g(r)$ for higher λ values changes to 1.4 for $\lambda = 5.36$ and to 1.3 for $\lambda = 6.17$, we do not observe any significant change in the result. In addition, for all bonding criteria we have observed same trend in the connectivity with λ.

C. Static structure factor

In order to study the extent of spatial correlations, we analyze the static structure factor $S(q)$ which is the density

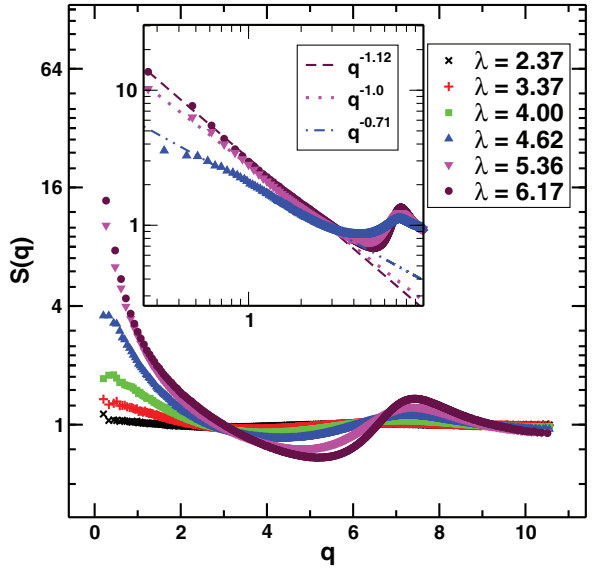

FIG. 3. (Color online) The static structure factor $S(q)$, at volume fraction $\phi = 0.007$, for systems with different λ values, in a log-linear plot. The inset shows the same data for dipole moments greater than 4.0 in a log-log plot with dashed lines showing the power-law behavior at small q values.

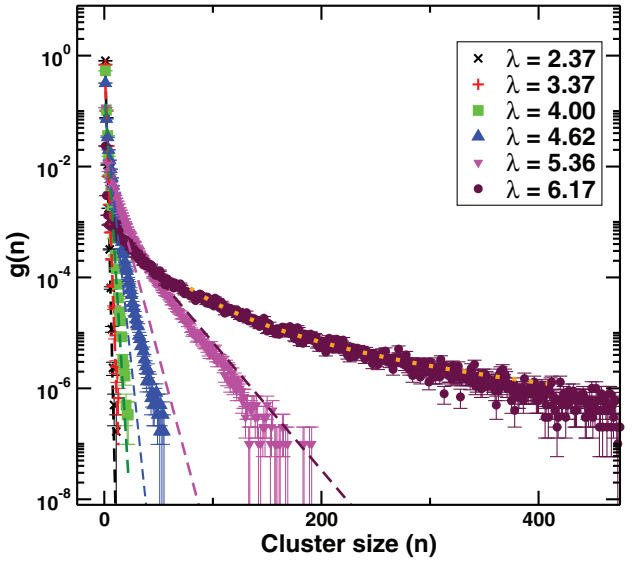

FIG. 4. (Color online) The cluster size distribution $g(n)$ as a function of cluster size n, at volume fraction $\phi = 0.007$, for systems having different λ values, in a log-log plot. The exponential fit to simulation data is indicated by dashed lines. The power-law fit to the cluster size distribution of the system at $\lambda = 6.17$ is shown in dotted lines.

correlation function in Fourier space, defined as [52]

$$S(q) = \frac{1}{N}\sum_j \sum_k \langle \exp(-i\mathbf{q}\cdot(\mathbf{r}_j - \mathbf{r}_k)\rangle, \tag{7}$$

where $\mathbf{q}$ is the wave vector and $q = |\mathbf{q}|$. As observed in the pair correlation function, $S(q)$ also shows gaslike behavior in the weakly interacting regime. The large-length-scale characteristics of $S(q)$ change with increasing λ value and show a power-law behavior beyond λ_t in the regime $0.26 < q < 4.0$. It is known that the static structure factor scales as $S(q) \sim q^{-d}$, where d is the fractal dimension of clusters and for rodlike molecules $d = 1$ [57]. The transient nature of the power-law exponent d is shown in Fig. 3. Exponents d less than 1 have been interpreted as showing a crossover region to a gel-like regime [58,59]. A similar scaling behavior of $S(q)$ has been found in strongly interacting dipolar colloids with moderate volume fraction [47,60]. In our study, we find larger amplitudes of $S(q)$ at low q even for λ values less than those used in the above works. We have verified that the scaling behavior does not change with system size in the range of $N = 1000$ to $N = 8000$ particles. We therefore conclude that these large-scale structures are quite sensitive to the concentration.

D. Cluster size distribution

We investigate the structure formation of dipolar colloids by monitoring the cluster size distribution $g(n)$, which gives information on the number of large clusters in the system. The particles are considered to be in the same cluster according to the same criterion that has been considered to find the connectivity. We find that the cluster size distribution below λ_t is described by an exponential decay. This observation agrees with the prediction of the chain model [14,61] that the chain size distribution decays exponentially as given by $g(n) \propto \exp(-n/\langle n\rangle)$, where n is the number of particles in a cluster and $\langle n\rangle$ is the average cluster size. The latter is true only when the average chain size is much larger than 1. For the general case we fit the chain size distribution by $g(n) \propto \exp(-n/a_0)$, where the average chain size $\langle n\rangle = [1 - \exp(-1/a_0)]^{-1}$.

From Fig. 4, it is evident that the average cluster size increases with interaction strength, and we see larger clusters than those reported in a simulation study by Wang *et al.* [17], where the volume fraction is higher than that we study in this work. At higher λ values, the cluster size distribution deviates from exponential decay behavior and the tail region follows a power law $g(n) = n^{-\nu}$ with an exponent $\nu \approx 2.4$. In the presence of a percolating cluster, in a three-dimensional system, the exponent ν can vary in the range $2 < \nu < 5/2$ [57]. In colloidal gels, the exponent value is found to be 2.2 [58]. We have observed the node-forming ability of the system from the other structural quantities; the power-law exponent ν from the cluster size distribution also supports this observation.

We calculate $\langle n\rangle$ as described in the chain model for the zero-field case as a function of λ [15],

$$\langle n\rangle = \frac{1}{2} + \left(\frac{1}{4} + \phi\frac{\exp(2\lambda)}{3\lambda^3}\right)^{1/2}. \tag{8}$$

We compare the result with $\langle n\rangle$ both from simulation and from the exponential fit to simulation data which is shown in Fig. 5. We find that the theoretical prediction underestimates the average cluster size at higher λ values due to the lack of interchain interactions. We could clearly observe in simulations the node-forming ability of the system; thus we conclude that interchain interactions cannot be neglected in getting full information on the structural properties of the system.

In Fig. 6, we show snapshots of the system for various λ values. Particles are colored according to the number of

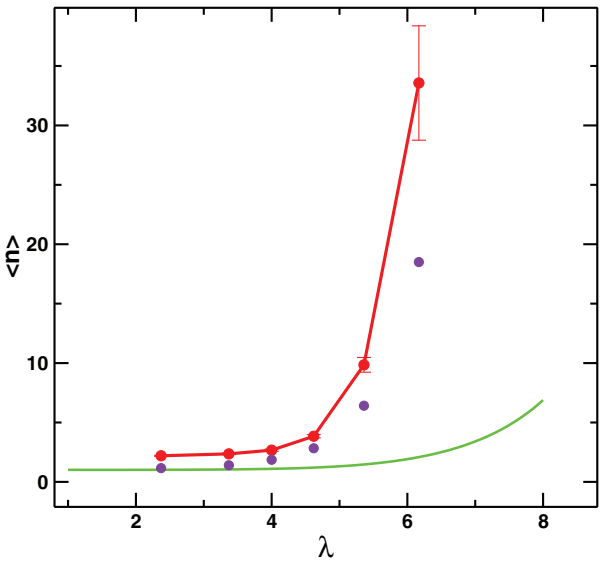

FIG. 5. (Color online) Average cluster size $\langle n \rangle$, at volume fraction $\phi = 0.007$, for systems with different λ values. The red data points show the average cluster size obtained from simulations. The green smooth curve is the prediction from the chain model. The filled violet circles indicate the average cluster size obtained from the exponential fit to simulation data.

neighbors. Isolated particles are colored gray; particles having one and two neighbors are shown in red (shaded dark in off-line version) and these particles participate in chain formation. We observe also particles with more than two neighbors which are colored green (shaded light in off-line version). These particles form nodes that connect chains and thereby create networklike structures. It is evident from the different snapshots of the system that there is no columnar structure [62] formation, for which the static structure factor is entirely different from the one we obtained in our system. Our system shows similar static structure factor characteristics as observed in gel systems or in systems having spanning clusters [54–56].

In order to understand the zero-field properties of ferrofluids, we studied the structural properties and found a crossover region in terms of the dipolar interaction strength. This crossover region helps in understanding the structural transitions of ferrofluids, and we focus in the following on dynamic properties to gain further insight into this crossover region.

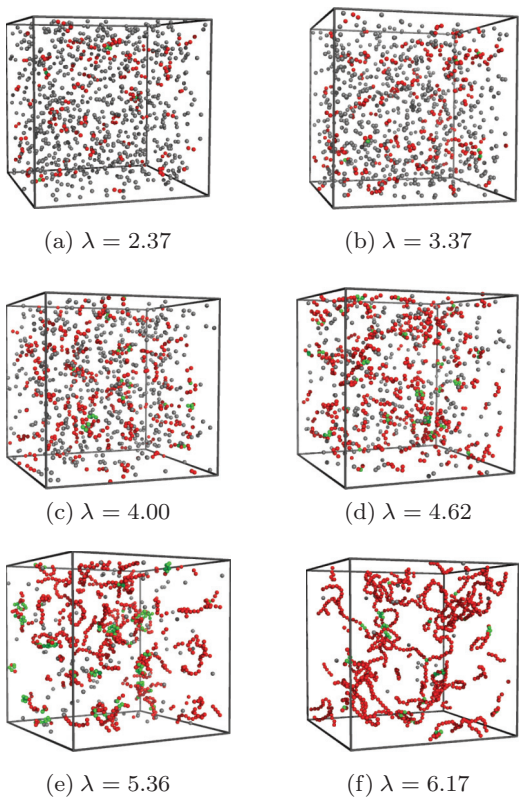

(a) $\lambda = 2.37$ (b) $\lambda = 3.37$

(c) $\lambda = 4.00$ (d) $\lambda = 4.62$

(e) $\lambda = 5.36$ (f) $\lambda = 6.17$

FIG. 6. (Color online) Snapshots of the system, at volume fraction $\phi = 0.007$, with different λ values. The color coding is explained in the text.

IV. DYNAMIC PROPERTIES

The Langevin dynamics given by Eqs. (3) and (4) allows us to study also dynamical properties, in particular, the diffusion coefficients (from the mean square displacement and the orientational correlation function), the structural relaxation time (from the incoherent scattering function), and the shear viscosity (from the stress correlation function) for different dipolar interaction strengths in the absence of hydrodynamic interactions (we expect that these interactions will not play a significant role due to the very low density of the system [29]). We also attempt to understand the change in dynamics in terms of the underlying change in structure.

A. Diffusion

The single-particle translational diffusion can be traced by calculating the mean square displacement (MSD) of particles which is defined as [52]

$$\langle r^2(t) \rangle = \frac{1}{N} \sum_{i=1}^{N} \langle |\mathbf{r}_i(t) - \mathbf{r}_i(0)|^2 \rangle, \tag{9}$$

where $\mathbf{r}_i(t) - \mathbf{r}_i(0)$ is the displacement vector of particle i over a time interval t. In order to improve the statistics, we average the MSD over different time origins.

The translational self-diffusion coefficient D_{trans} is obtained from the slope of the long-time regime of the mean square displacement using the Einstein formula given by

$$D_{\text{trans}} = \lim_{t \to \infty} \frac{\langle r^2(t) \rangle}{6t}. \tag{10}$$

We find that below λ_t the translational diffusion coefficient decreases with increasing λ, similar to Arrhenius behavior. But a dramatic decrease is observed beyond λ_t (Fig. 7). This sudden decrease in D_{trans} has not been observed in systems having higher volume fractions [26–28,31,63,64]. As discussed in the previous section, beyond λ_t, we find an increase in the population of two-coordinated and three-coordinated particles that form elongated chains or connected structures.

We also explored the effect of dipolar interaction strength on the rotational diffusion. We extract the rotational diffusion coefficient D_{rot} from the orientational autocorrelation function

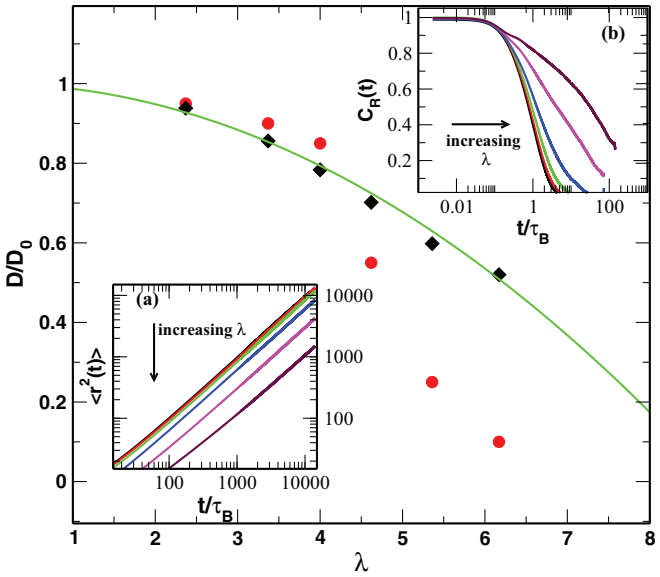

FIG. 7. (Color online) The scaled diffusion coefficients D/D_0 for translational and rotational dynamics ($D_{\rm trans}/D_0$ and $D_{\rm rot}/D_0$) for different λ values at volume fraction $\phi = 0.007$. D_0 is the bare diffusion coefficient defined as $D_0 = k_{\rm B}T/\xi$, where ξ is $\xi^{\rm T}$ for translational dynamics and $\xi^{\rm R}$ for rotational dynamics. The filled circles and diamonds represent the translational and the rotational diffusion coefficients, respectively. The continuous curve is the quadratic fit to the rotational diffusion coefficient. The inset (a) shows the mean square displacement [Eq. (9)] and the inset (b) shows the orientational correlation function [Eq. (11)] for different λ values between 2.37 and 6.17.

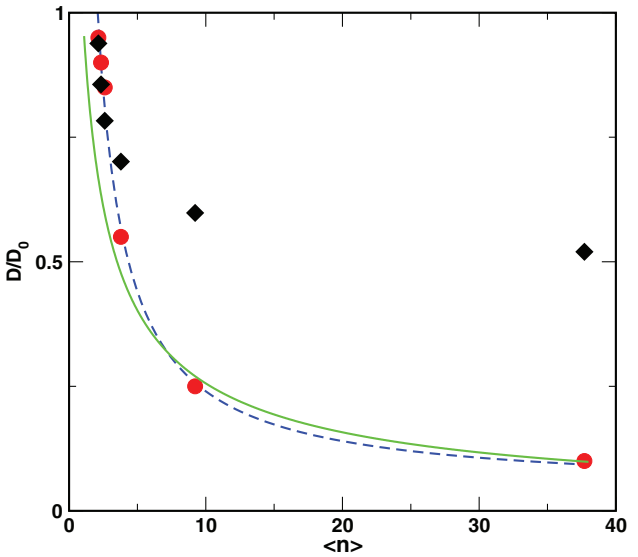

FIG. 8. (Color online) The translational and rotational diffusion coefficients as functions of average cluster size $\langle n\rangle$. The circles represent the translational diffusion coefficient and the diamonds represent the rotational diffusion coefficient. The continuous green curve is from the chain model prediction. The dashed curve is a fit of the form $D_{\rm trans}/D_0 = 2/\langle n\rangle$.

$C_{\rm R}(t)$ of dipole moments which is defined as [50]

$$C_{\rm R}(t) = (1/N)\left\langle \sum_i \mathbf{u}_i(t)\cdot\mathbf{u}_i(0)\right\rangle. \qquad (11)$$

For short times, the orientational correlation function decays exponentially, $C_{\rm R}(t) \sim \exp(-2D_{\rm rot}t)$. The rotational diffusion coefficient extracted from the orientational autocorrelation function is shown as diamond symbols in Fig. 7. We find that the rotational diffusion coefficient decreases with increasing dipolar interaction strength. This feature has not been observed in previous experimental and simulation studies of magnetic fluids with weak dipolar interaction [65,66]. We find that the dependence of $D_{\rm rot}$ on λ fits a quadratic function of the form $D_{\rm rot}/D_0 = 1.0 - A_0\lambda^2$, which is in agreement with the theoretical calculation of the rotational diffusion coefficient of ferrofluids [27].

We show in Fig. 8 the translational and rotational diffusion coefficients as functions of the average chain size, which clearly shows that the structural formation causes a slowing down of the dynamics of the system. According to the chain model, the translational diffusion coefficient decays as $D_{\rm trans}/D_0 = \ln\langle n\rangle/\langle n\rangle$, which is shown as the continuous green curve in Fig. 8. As can be seen, the chain model predicts qualitatively the trend of $D_{\rm trans}$ with change in the chain size. We find that the translational diffusion coefficient varies as $2/\langle n\rangle$, which describes collective diffusion of the particles in a chain by addition of the diffusion coefficients of each particle belonging to the chain. The factor of 2 comes from the simple assumption that the translational diffusion of small chains (two particles per chain) matches single-particle diffusion (see the dashed curve in Fig. 8). The rotational diffusion coefficient also decreases with increasing interaction strength. But there is no dramatic decrease in $D_{\rm rot}$ such as we observe in $D_{\rm trans}$.

B. Incoherent scattering function

We obtain information about single-particle dynamics at various length scales by computing the incoherent scattering function $F_{\rm s}(q,t)$, which can also be obtained in scattering experiments, defined as [52]

$$F_{\rm s}(q,t) = \frac{1}{N}\sum_{i=1}^{N}\langle\exp\{-i\mathbf{q}\cdot[\mathbf{r}_i(t) - \mathbf{r}_i(0)]\}\rangle. \qquad (12)$$

To begin with we study the behavior of $F_{\rm s}(q,t)$ at the q value corresponding to the first peak of $S(q)$ ($q \sim 7$) for various λ values. We find that at these short length scales, the relaxation times $\tau(q)$—obtained either from the exponential fit or by taking the time which corresponds to $F_{\rm s}(q,t) = 1/e$—do not change considerably with the interaction strength [$\tau(q)/\tau_{\rm B} = 0.3300(\pm0.0003) - 0.390(\pm0.014)$]. As noted before, for interaction strengths beyond $\lambda_{\rm t}$ we find structural changes which include long chains and node-forming particles and hence it would be interesting to look at the q dependence of $F_{\rm s}(q,t)$.

For $\lambda = 6.17$, we show in Fig. 9 the behavior of $F_{\rm s}(q,t)$ for different q values. We find that with a decrease in q value, the relaxation times are increasing and also the decay of $F_{\rm s}(q,t)$ follows a stretched exponential behavior (discussed below). For different interaction strengths, the variation of relaxation time at $q = 0.29$ (half of the box length) is shown in Fig. 10. We find for λ greater than $\lambda_{\rm t}$ a rapid increase in the relaxation time which is due to the presence of slowly relaxing structures.

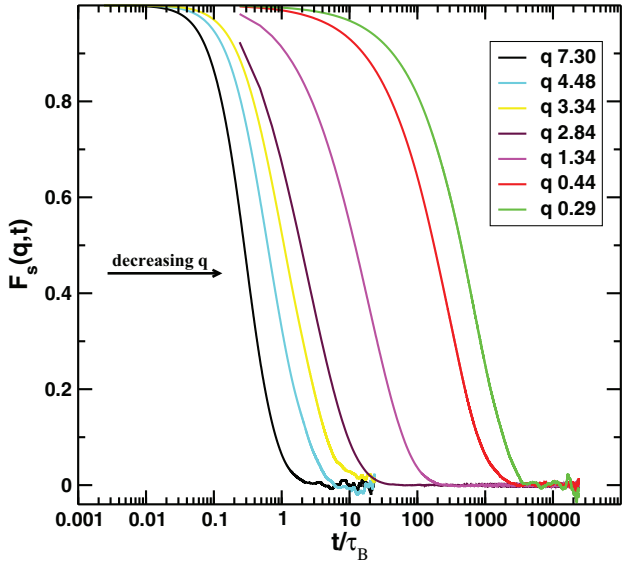

FIG. 9. (Color online) The incoherent scattering function $F_s(q,t)$ for the system having $\lambda = 6.17$ for different wave vectors.

The $F_s(q,t)$ curves are fitted well by the Kohlrausch-Williams-Watts (KWW) form which is given by $F_s(q,t) = A\exp\{-[t/\tau(q)]^\beta\}$ where A is a constant, τ is the relaxation time, and β is the KWW exponent. We find that at large length scales the value of β changes from single exponential ($\beta = 1.000 \pm 0.009$) to stretched ($\beta = 0.84 \pm 0.02$) exponential behavior as λ varies from 2.37 to 6.17. The single exponential decay results from normal Arrhenius behavior of the density correlation function, whereas stretched exponential decay is due to the presence of structures having different relaxation times which slow down the overall dynamics. Thus the average relaxation time corresponding to the KWW form is

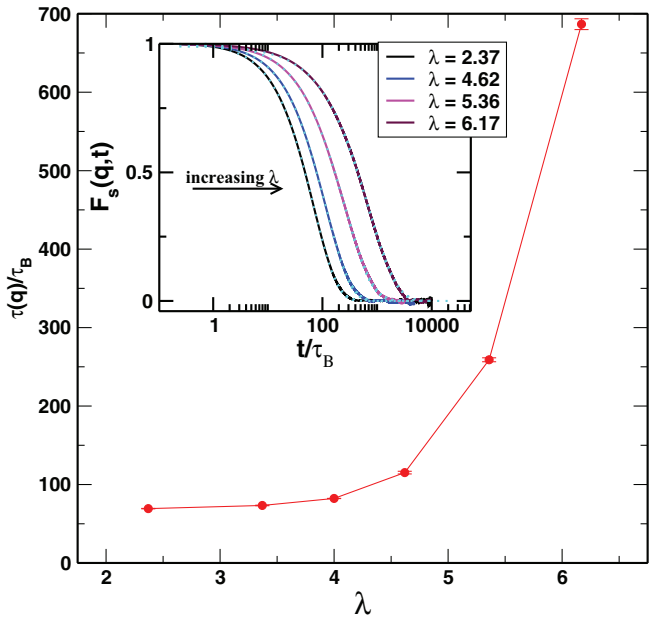

FIG. 10. (Color online) The relaxation time $\tau(q)$ at large length scales for different λ values. The inset shows the large-length-scale behavior of $F_s(q,t)$.

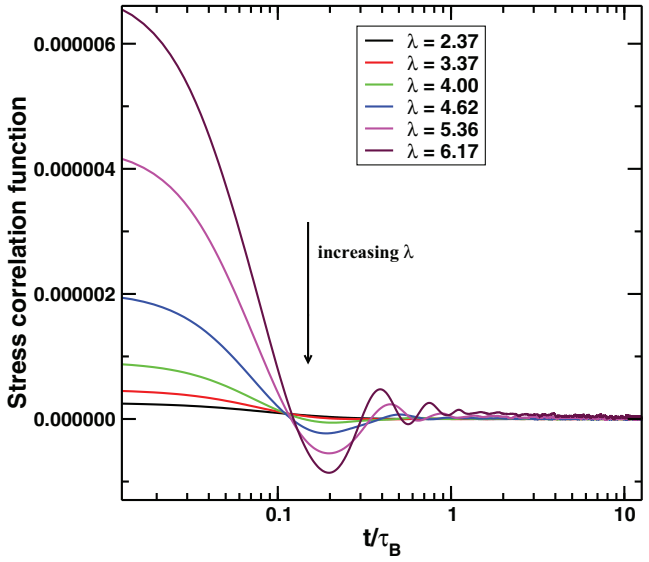

FIG. 11. (Color online) The time-dependent stress correlation function, at volume fraction $\phi = 0.007$, for different λ values.

defined by

$$\langle\tau\rangle = \int_0^\infty \exp\{-[t/\tau(q)]^\beta\}dt.$$

We find that the average relaxation time $\langle\tau\rangle$ matches $\tau(q)$ calculated from $F_s(q,t)$ up to the crossover dipolar interaction strength λ_t. The deviation of $\langle\tau\rangle$ from $\tau(q)$ beyond λ_t is related to the stretched exponential decay of $F_s(q,t)$. The KWW form of $F_s(q,t)$ is also observed in gel- and glass-forming systems [54,67].

C. Viscosity

We calculate the shear viscosity η, which is related to the rate of momentum transport through the system, using the Green-Kubo formula [48]

$$\eta = \frac{V}{k_B T}\int_0^\infty \langle\sigma_{xy}(t)\sigma_{xy}(0)\rangle dt, \tag{13}$$

where σ_{xy} is the off-diagonal element of the stress tensor,

$$\sigma_{xy} = \frac{1}{V}\left(\sum_{i<j}^{N} r_{ijx} f_{ijy} + \sum_{i=1}^{N}\frac{p_{ix}p_{iy}}{M}\right), \tag{14}$$

where $\mathbf{f}_{ij}$ is the force exerted on particle i by particle j and $\mathbf{p}_i(t) = M\mathbf{v}_i(t)$.

The stress correlation function $\langle\sigma_{xy}(t)\sigma_{xy}(0)\rangle$ for systems with different interaction strengths (Fig. 11) shows that the amplitude of the correlation increases with increasing λ in the short-time regime. A significant long-time tail develops beyond λ_t, indicating a sustaining stress in the system. The long tail has to be integrated correctly to get an accurate value of η.

We calculate the viscosity from Eqs. (13) and (14). Further, we investigate the viscosity change with dipolar interaction strength and with chain size. In Fig. 12, it is shown that the viscosity increases linearly with chain size, $\eta/\eta_s = 1 + A_1\langle n\rangle$ (dashed curve in the bottom panel). The viscosity change with

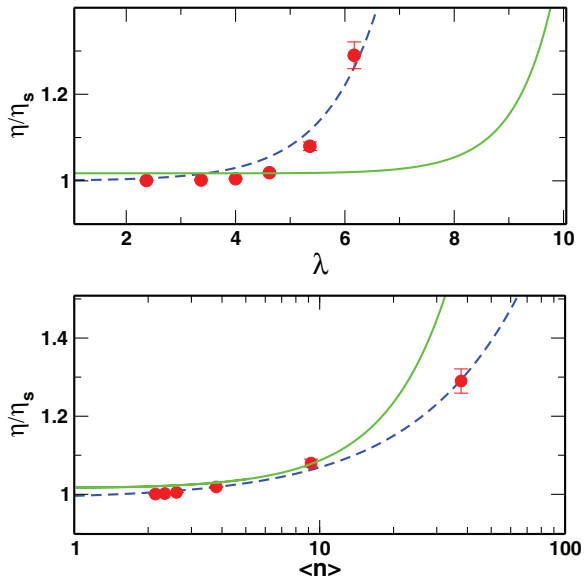

FIG. 12. (Color online) The viscosity for different λ values at volume fraction $\phi = 0.007$ is shown in the top panel. In the bottom panel, the viscosity is plotted as a function of chain size. The data points show the simulation results and the continuous green curves are from the chain model. The blue dashed curves are fitting functions to the data (given in the text).

dipolar interaction strength shows an exponential behavior at higher λ values and the data points more or less have a similar trend as the function $\eta/\eta_s = 1 + A_2 \exp(\lambda)$ (dashed curve in the top panel). Further, we compare the viscosity results with the theoretical prediction by Zubarev and Iskakova [14,41], which is based on the assumptions that chains are considered to be straight and rigid and the interchain interactions are neglected. The chain model prediction for viscosity in the absence of field and flow is given by

$$\frac{\eta}{\eta_s} = 1 + \sum_n 5\phi_n \left(Q_1 + \frac{2}{3} Q_3 - \frac{2}{15} Q_{23} \right), \qquad (15)$$

where ϕ_n is the volume fraction of n-particle chains. In the chain model, each chain is modeled as a rigid ellipsoid with an axis ratio n equal to the chain size. The coefficients Q_i depend only on the axis ratios of the ellipsoids which are given in the Appendix. Due to these assumptions, we observe that the theoretical model overpredicts the influence of chain size and underpredicts the influence of dipolar interaction strength on viscosity (continuous curve in both panels).

The reaction field approach contributes to the calculation of the torque due to long-range dipole-dipole interaction but it does not contribute to the calculation of the force, and consequently there is no contribution to the stress tensor either. To overcome this approximation, we have chosen a very large cutoff for the reaction field, $r_{RF} = 8\sigma$, which is nearly half of the box length, so that it does not affect the stress relaxation and the viscosity of our system. We have cross-checked the results with a larger cutoff than this and have found no visible change in the viscosity and the stress correlation function.

V. CONCLUSIONS

In this work we study the structural and dynamic properties of dilute magnetic colloids by varying the dipolar interaction strength using Langevin dynamics simulations. We parametrize the interaction potential to mimic the cobalt-based nanoparticles that are used in experiments [42]. The strength of the interaction is further varied (below and above the values corresponding to that which mimic the experiments) in this study. From the structural analysis we observe the formation of complex microstructures which constitute chains and node-forming structures. The dynamics of the system show a slowing down at higher interaction strength. We find that the structural and dynamic crossovers happen at around the same interaction strength, and a systematic connection between the structure and dynamics of the system is observed. The existing theoretical model qualitatively predicts the trend of changes in the diffusion coefficient and viscosity with increase in chain size, but a clear quantitative difference is observed at larger values of interaction strength, where we find a steep increase in the zero-shear viscosity in a narrow range of dipolar interaction strengths. We hope that the present study can give hints toward improving the theoretical modeling of dilute and interacting ferrofluids.

ACKNOWLEDGMENTS

We are grateful to Hans Christian Öttinger at ETH Zürich and S. Odenbach, J. Linke, and D. Borin at Technical University, Dresden for interesting and valuable discussions. We acknowledge Pieter J. in't Veld at BASF SE, Germany for technical support in implementing the Ewald sum method for dipolar fluids. We are grateful to the Swiss National Science Foundation (SNSF) for funding this Project No. 20PA21E-129506: "Experiment and Computer Simulation of the Anisotropy of the Magnetoviscous Effect."

APPENDIX

The geometric coefficients occurring in the viscosity formula of the chain model are given by [14,41]

$$Q_0 = \frac{2(n^2-1)^2}{5n^2(2n^2\beta - \beta - 1)}, \qquad (A1)$$

$$Q_1 = \frac{4(n^2-1)^2}{5n^2(3\beta + 2n^2 - 5)}, \qquad (A2)$$

$$Q_2 = \frac{Q_1}{3}\left[1 - \frac{2n^2 + 1 - (4n^2-1)\beta}{4(2n^2+1)\beta - 13}\right], \qquad (A3)$$

$$Q_3 = Q_1\left[\frac{[n^2(\beta+1) - 2](3\beta + 2n^2 - 5)}{4[\beta(2n^2-1) - 1](n^2 + 2 - 3n^2\beta)} - 1\right], \qquad (A4)$$

where $\beta = \frac{1}{n\sqrt{|n^2-1|}} \cosh^{-1}(n)$, for $n > 1$, and

$$Q_{23} = 3Q_2 + 4Q_3.$$

[1] C. Scherer and A. M. F. Neto, Braz. J. Phys. **35**, 718 (2005).
[2] K. Raj, B. Moskowitz, and R. Casciari, J. Magn. Magn. Mater. **149**, 174 (1995).
[3] V. Cabuil, Curr. Opin. Colloid Interface Sci. **5**, 44 (2000).
[4] F. Cousin, E. Dubois, and V. Cabuil, Phys. Rev. E **68**, 021405 (2003).
[5] C. F. Tejero, A. Daanoun, H. N. W. Lekkerkerker, and M. Baus, Phys. Rev. Lett. **73**, 752 (1994).
[6] S. Hachisu, Y. Kobayashi, and A. Kose, J. Colloid Interface Sci. **42**, 342 (1973).
[7] H. Lekkerkerker, W. Poon, P. Pusey, A. Stroobants, and P. Warren, Europhys. Lett. **20**, 559 (1992).
[8] P. G. de Gennes and P. A. Pincus, Phys. Kondens. Mater. **11**, 189 (1970).
[9] P. C. Jordan, Mol. Phys. **25**, 961 (1973).
[10] P. C. Jordan, Mol. Phys. **38**, 769 (1979).
[11] H. Zhang and M. Widom, Phys. Rev. E **51**, 2099 (1995).
[12] M. A. Osipov, P. I. C. Teixeira, and M. M. Telo da Gama, Phys. Rev. E **54**, 2597 (1996).
[13] I. Pérez-Castillo, A. Pérez-Madrid, J. M. Rubi, and G. Bossis, J. Chem. Phys. **113**, 6443 (2000).
[14] A. Y. Zubarev and L. Y. Iskakova, Phys. Rev. E **61**, 5415 (2000).
[15] K. I. Morozov and M. I. Shliomis, J. Phys.: Condens. Matter **16**, 3807 (2004).
[16] V. S. Mendelev and A. O. Ivanov, Phys. Rev. E **70**, 051502 (2004).
[17] Z. Wang, C. Holm, and H. W. Müller, Phys. Rev. E **66**, 021405 (2002).
[18] Z. Wang and C. Holm, Phys. Rev. E **68**, 041401 (2003).
[19] J. M. Tavares, J. J. Weis, and M. M. Telo da Gama, Phys. Rev. E **65**, 061201 (2002).
[20] H. Morimoto and T. Maekawa, J. Phys. A **33**, 247 (2000).
[21] S. Hess, J. B. Hayter, and R. Pynn, Mol. Phys. **43**, 1527 (1985).
[22] C. Holm and J. J. Weis, Curr. Opin. Colloid Interface Sci. **10**, 133 (2005).
[23] B. Huke and M. Lücke, Rep. Prog. Phys. **67**, 1731 (2004).
[24] L. Rovigatti, J. Russo, and F. Sciortino, Phys. Rev. Lett. **107**, 237801 (2011).
[25] G. Ganzenmüller, G. Patey, and P. J. Camp, Mol. Phys. **107**, 403 (2009).
[26] M.Hernández-Contreras, P.González-Mozuelos, O. Alarcón-Waess, and H. Ruíz-Estrada, Phys. Rev. E **57**, 1817 (1998).
[27] M. Hernández-Contreras and H. Ruíz-Estrada, Phys. Rev. E **68**, 031202 (2003).
[28] P. Ilg and M. Kröger, Phys. Rev. E **72**, 031504 (2005).
[29] E. Kim, K. Stratford, P. Camp, and M. Cates, J. Phys. Chem. B **113**, 3681 (2008).
[30] L. Y. Iskakova and A. Y. Zubarev, Phys. Rev. E **66**, 041405 (2002).
[31] P. Ilg, Phys. Rev. E **71**, 051407 (2005).
[32] S. Odenbach, *Magnetoviscous Effects in Ferrofluids*, Lecture Notes in Physics Vol. 71 (Springer, Berlin, 2002).
[33] E. Uhlmann and N. Bayat, Product. Eng. **10**, 125 (2003).
[34] A. Kose, B. Fischer, L. Mao, and H. Koser, Proc. Natl. Acad. Sci. U.S.A. **106**, 21478 (2009).
[35] M. Zahn, J. Nanopart. Res. **3**, 73 (2001).
[36] C. Alexiou, R. Jurgons, C. Seliger, O. Brunke, H. Iro, and S. Odenbach, Anticancer Res. **27**, 2019 (2007).
[37] S. Odenbach and K. Raj, Magnetohydrodynamics **36**, 379 (2000).
[38] A. Mertelj, A. Rešetič, S. Gyergyek, D. Makovec, and M. Čopič, Soft Matter **7**, 125 (2010).
[39] J. P. McTague, J. Chem. Phys. **51**, 133 (1969).
[40] P. Ilg, M. Kröger, and S. Hess, Phys. Rev. E **71**, 051201 (2005).
[41] P. Ilg and S. Odenbach, in *Colloidal Magnetic Fluids: Basics, Development and Applications of Ferrofluids*, edited by S. Odenbach, Lecture Notes in Physics Vol. 763 (Springer, Berlin, 2008).
[42] M. Gerth-Noritzsch, D. Yu Borin, and S. Odenbach, J. Phys.: Condens. Matter **23**, 346002 (2011).
[43] A. Satoh, R. W. Chantrell, G. N. Coverdale, and S. Kamiyama, J. Colloid Interface Sci. **203**, 233 (1998).
[44] A. Satoh, R. W. Chantrell, and G. N. Coverdale, J. Colloid Interface Sci. **209**, 44 (1999).
[45] H. Morimoto and T. Maekawa, Int. J. Mod. Phys. B **15**, 823 (2001).
[46] H. Morimoto, T. Maekawa, and Y. Matsumoto, Phys. Rev. E **65**, 061508 (2002).
[47] J. P. Huang, Z. W. Wang, and C. Holm, Phys. Rev. E **71**, 061203 (2005).
[48] M. P. Allen and D. J. Tildesley, *Computer Simulation of Liquids* (Oxford University Press, Oxford, 1987).
[49] A. Sreekumari, P. J. in't Veld, and P. Ilg (unpublished).
[50] J. K. G. Dhont, *An Introduction to Dynamics of Colloids*, Studies in Interface Science (Elsevier, Amsterdam, 1996).
[51] S. Plimpton, J. Comput. Phys. **117**, 1 (1995).
[52] J. Hansen and I. McDonald, *Theory of Simple Liquids* (Academic Press, London, 2006).
[53] R. Blaak, M. Miller, and J. Hansen, Europhys. Lett. **78**, 26002 (2007).
[54] P. Ilg and E. Del Gado, Soft Matter **7**, 163 (2010).
[55] L. Rovigatti, J. Russo, and F. Sciortino, Soft Matter **8**, 6310 (2012).
[56] S. Saw, N. L. Ellegaard, W. Kob, and S. Sastry, J. Chem. Phys. **134**, 164506 (2011).
[57] D. Stauffer and A. Aharony, *Introduction to Percolation Theory* (CRC, Boca Raton, FL, 1994).
[58] E. Del Gado and W. Kob, Soft Matter **6**, 1547 (2010).
[59] M. Carpineti and M. Giglio, Phys. Rev. Lett. **68**, 3327 (1992).
[60] E. Pyanzina, S. Kantorovich, J. Cerdà, A. Ivanov, and C. Holm, Mol. Phys. **107**, 571 (2009).
[61] A. Y. Zubarev and L. Y. Iskakova, JETP **80**, 857 (1995).
[62] P. Ilg, Eur. Phys. J. E **26**, 169 (2008).
[63] K. Morozov, J. Magn. Magn. Mater. **122**, 98 (1993).
[64] J. Jordanovic, S. Jäger, and S. H. L. Klapp, Phys. Rev. Lett. **106**, 038301 (2011).
[65] G. Mériguet, E. Dubois, M. Jardat, A. Bourdon, G. Demouchy, V. Dupuis, B. Farago, R. Perzynski, and P. Turq, J. Phys.: Condens. Matter **18**, S2685 (2006).
[66] G. Mériguet, M. Jardat, and P. Turq, J. Chem. Phys. **123**, 144915 (2005).
[67] W. Kob and H. C. Andersen, Phys. Rev. Lett. **73**, 1376 (1994).